DNA-Directed Self-Assembly of Gold Nanoparticles onto Nanopatterned Surfaces: Controlled Placement of Individual Nanoparticles into Regular Arrays

Cecilia H Lalander,[†] Yuanhui Zheng,[‡] Scott Dhuey,[§] Stefano Cabrini,[§] and Udo Bach[†,‡,*]

[†]School of Chemistry and [‡]Department of Materials Engineering, Monash University, Wellington Road, Clayton, VIC 3800, Australia and [§]Molecular Foundry, Lawrence Berkeley National Laboratories, 1 Cyclotron Road, Berkeley, CA, 94720, United States

ABSTRACT A method for the templated DNA-directed self-assembly of individual gold nanoparticles (AuNPs) into discrete nanostructures is described. The templating nanostructures consisted of a linear configuration of six metal dots with a center-to-center dot distance of 55 nm, fabricated by means of electron beam lithography. The 40 nm DNA-capped AuNPs were immobilized onto this templating nanostructure to produce a linear configuration of six adjacent AuNPs. The geometry of the templating nanostructure was found to be critically important for the successful direction of a single nanoparticle onto individual adsorption sites. For optimized template structures the immobilization efficiency of nanoparticles onto the individual adsorption sites was found to be 80%. The nonspecific association of nanoparticles with specifically adsorbed nanoparticles and the between adsorption of nanoparticles, bridging two individual adsorption sites, were the two main defects observed in the immobilized assemblies. Less than 1% of all surface confined AuNPs adsorbed nonspecifically in the areas between the self-assembled regular arrays.

KEYWORDS: nanopattern · DNA-directed · templated · self-assembly · gold nanoparticles · arrays

The resolution limits of conventional top-down lithographic fabrication techniques have steadily improved over the last decades. As a result, sub-100 nm fabrication technologies have now become new standards in the semiconductor device industry. The rate of progress, however, cannot be maintained, as fundamental thermodynamic limits are being reached.[1] The next generation of lithography tools attempt to circumvent these fundamental limits but with a remarkable increase in production cost.[2] These hurdles have motivated the exploration of novel and more unconventional nanofabrication techniques.[3,4] Bottom-up assembly strategies involving the self-assembly of small building blocks (*e.g.*, molecules and nanoparticles) to form more complex nanostructures are currently being explored as alternative nanofabrication tools. Chemical synthesis allows for the production of bulk quantities of multicomponent nanoparticle building blocks, monodisperse in size, in a variety of shapes. Structures well beyond 1 nm, (*e.g.*, the shell thickness in core−shell nanoparticles)[5] can be synthesized, which is well outside the scope of any lithographic method.

Although conversely, it remains uncertain whether such bottom-up assembly strategies alone will be successful in producing complex devices, such as electronic or plasmonic circuits with macroscopic dimensions. A more likely scenario is that bottom-up techniques will be used as complementary process steps within a sequence of classical top-down fabrication methods.[6−11] The integration of synthetically produced nanostructures into lithographically produced structures would allow for the exploitation of their unique properties that result from their refined nanostructure.[12−15] Furthermore, chemically prepared single-crystalline metal nanoparticles were shown to exhibit dramatically reduced surface plasmon damping, compared to lithographically fabricated nanostructures, qualifying them as ideal building blocks for plasmonic applications.[16,17]

Controlled self-assembly is required to achieve this and ultimately demands for self-assembly techniques that allow to direct individual nanoparticles onto predefined surface sites. Combining chemical nanoparticle synthesis and advanced bottom-up self-assembly strategies with

*Address correspondence to udo.bach@sci.monash.edu.au.

Received for review June 24, 2010 and accepted September 15, 2010.

Published online October 8, 2010. 10.1021/nn101431k

conventional top-down lithographic techniques would enable the assembly of nanoparticles with unique optical,[18−20] electronic,[21,22] and photovoltaic[23,24] properties into predefined formations (tetrapots,[25−27] superlattices,[28,29] barcode-like,[30,31] and pyramidal[32] structures).

Gold nanoparticles (AuNPs) have received a great deal of attention in the past decade due to their interesting optical properties[33,34] and are thus attractive candidates for use in optical devices, where the optical coupling ability of AuNPs[35] is exploited for signal transfer.[36] The plasmonic coupling of AuNPs is strongly dependent on the interparticle distance,[37,38] making it a critical parameter to control when fabricating plasmonic structures.

The self-assembly of nanoparticles onto surface patterns can be driven by a number of processes, such as electrostatic interaction, chemical binding, and hydrophilic/hydrophobic interaction.[39−44] DNA-directed self-assembly is unmatched by other self-assembly techniques due to its unlimited programmability, which allows the encoding of specific adsorption sites for a multitude of different nanometer-sized building blocks.[6,7] This will be of great importance if the parallel self-assembly of a number of different nanoscale building blocks onto a common substrate is envisaged.

DNA-directed assembly of AuNPs into complex configurations in solution,[45−47] as well as onto surfaces,[48−50] has been reported. Although the DNA-assisted assembly of building blocks has been investigated for over a decade, the assembly of nanobuilding blocks into nanosized configurations, and onto nanopatterned arrays, in high yields still remains a key challenge. Zhang *et al.* reported on the difficulty of the templated assembly of individual DNA-capped AuNPs onto a two-dimensional DNA nanogrid, observing an overall single particle immobilization efficiency of roughly 60%.[50] Other research groups have reported on the assembly of AuNPs in solution. Both Claridge *et al.*[27] and Qin and Yung have reported the DNA-assisted AuNP assembly into dimers, trimers, and tetramers. Claridge and co-workers used branched DNA scaffolds to produce different tetramer structures and estimated that the assembly process yielded the desired structures with 9% efficiency. Recently, several groups reported the DNA-directed assembly of metal nanoparticles onto DNA origami.[51−53] Sharma *et al.*[53] achieved a yield of 91% when directing lipoic acid-mediated AuNP−DNA conjugates onto origami nanoarrays.

In this study we explore the possibility of directing individual nanoparticles onto single absorption sites by DNA-directed self-assembly. For the fabrication of nanoscale devices it will be crucially important to allow the assembly of nanoscale building blocks in close vicinity to each other. For this study a simple model system was chosen; self-assembling AuNPs with a 40 nm diameter onto electron beam lithography (EBL) crafted gold nanopatterns, directed by Watson−Crick base pairing. The immobilization efficiency was calculated, and the distribution of assembly configurations assessed. To the best of our knowledge, this is the first report of DNA-directed assembly of nanobuilding blocks onto lithographically defined nanopatterns of high resolution over a large area with great specificity.

The templating nanopattern consisted of a matrix of six-dot lines. The six-dot line structures were chosen as an arbitrary representation of potential plasmonic structures. A combination of adsorption site diameter and pitch (center-to-center distance of two adjacent adsorption sites) was selected that allowed to assemble single metal nanoparticles at high yield in close proximity (Supporting Information, Figures SI-1 and SI-2).

Two different templating nanopatterns architectures were studied: substrate A (sub-A) with elevated features and substrate B (sub-B) with negative surface features. In Scheme 1 the proposed method for the direction of AuNPs onto the templating nanopattern is schematically represented.

The nanopatterned substrates were fabricated by EBL (Scheme 1, 1) crafting the nanopattern arrays into the resist poly(methyl methacrylate) (PMMA), followed by the nanopattern development (Scheme 1, 2). A chromium (adhesive layer) and gold layer were evaporated onto sub-A immediately following the development (Scheme 1, 3a). To attain the negative surface features in sub-B, a 110 nm silicon oxide layer was grown on the silicon substrate prior to the PMMA deposition, the nanopattern was crafted into the PMMA, and the substrate was immersed into an ammonium bifluorid etchant buffer, transferring the nanopattern into the silicon oxide, followed by bimetal evaporation (Scheme 1, 3b). Subsequent lift-off yielded the gold nanopattern, comprising of a matrix of six-dot lines. An area of 1 mm^2 was patterned with a total of four million 6-dot line features. The nanopattern arrays were functionalized with thiol-terminated DNA strands (surface DNA) (Scheme 1, 4), and a linker strand, with the function of linking the AuNPs to the templating nanopattern structures, was hybridized onto the surface DNA (Scheme 1, 5). The linker DNA was a single-stranded oligonucleotide comprising of two segments of 15 base pairs: one complementary to the surface DNA and the other complementary to the particle DNA. In the final step, the AuNP−DNA conjugates were assembled onto the nanopatterns through hybridization of particle DNA to the sticky-end of the linker DNA (Scheme 1, 6). When the AuNP self-assembly process was conducted without a linker (omitting step 5 in Scheme 1), no immobilization of AuNPs onto the nanopattern was expected, as nothing would link the AuNPs to the nanopattern.

RESULTS AND DISCUSSION

Atomic force microscope (AFM) and scanning electron microscope (SEM) micrographs of the two nano-

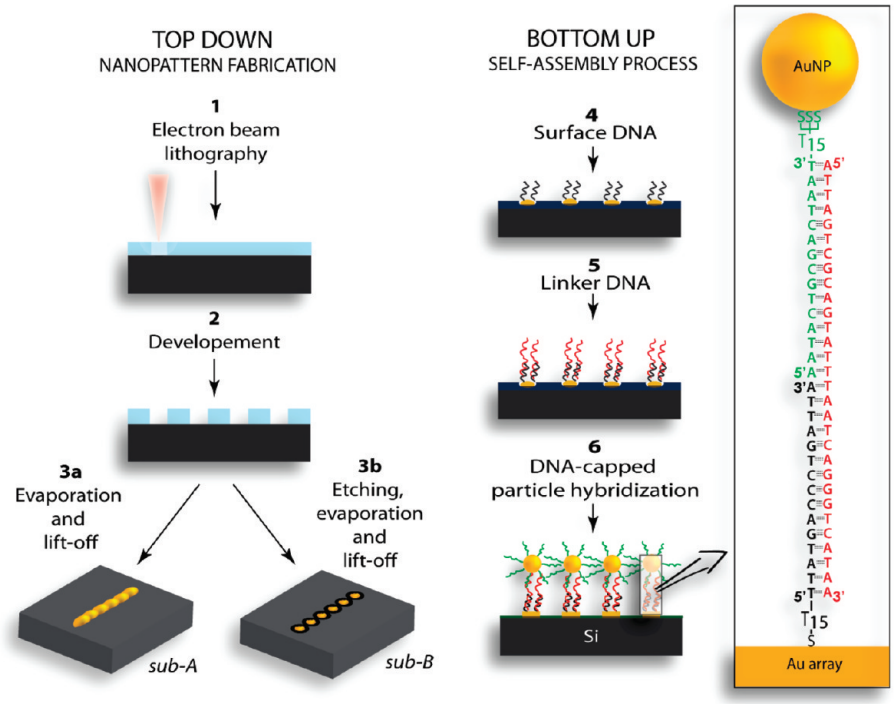

Scheme 1. Schematic Representation of Top-Down Nanopattern Fabrication and Bottom-Up Gold Nanoparticle Self-Assembly Process (Not to Scale)[a] [a](1) Nanopattern arrays crafted into PMMA by means of EBL; (2) pattern development; (3) etching (sub-B only), chromium and gold evaporation, and PMMA lift-off, yielding sub-A with elevated feature and sub-B with negative surface features, schematically illustrated; (4) gold nanopattern arrays functionalization with thiol-terminated surface DNA; (5) linker DNA hybridized onto surface DNA; and finally (6) AuNP−DNA conjugates were hybridized onto the templating nanopattern arrays. The inset show an illustration of the DNA interaction that drives the self-assembly, where the linker DNA (red in illustration) links the particle to the nanopattern array, as it comprises of two different 15 base-pair segments: one complementary to the surface DNA (black in illustration) and the other complementary to the particle DNA (blue in illustration, sticky-end).

pattern substrates, sub-A and sub-B, are displayed in Figure 1. The SEM and AFM micrographs shown in Figure 1 depict the two templating nanostructures: sub-A (A and B) and sub-B (C and D) yielded by top-down fabrication, displaying the remarkable precision of the fabrication method. The height of the features of sub-A

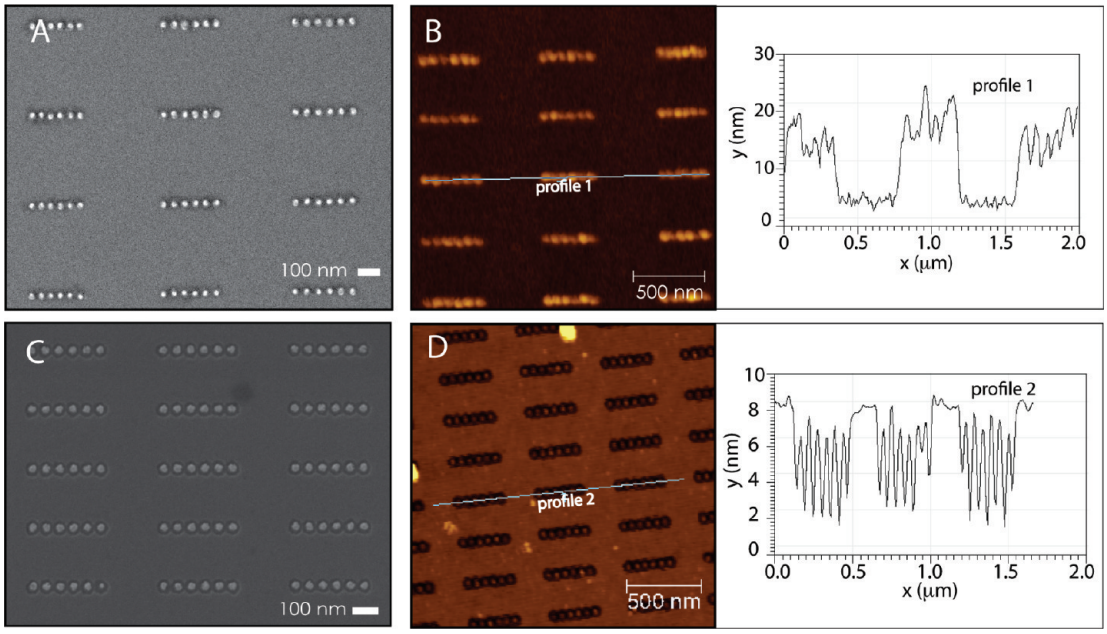

Figure 1. SEM and AFM micrographs displaying the architecture of the two nanopatterned substrates used for this study: (A) SEM micrograph of sub-A, (B) AFM micrograph and cross-section profile showing in more detail the six-dot lines that make up the templating nanopattern, with elevated features 15−18 nm high, (C) SEM micrograph of sub-B, (D) AFM micrograph and cross-section profile of sub-B, showing in closer detail the etched profiles containing six individual metal dots, located below the surface plain, evident as six local maxima in the cross-sectional profile.

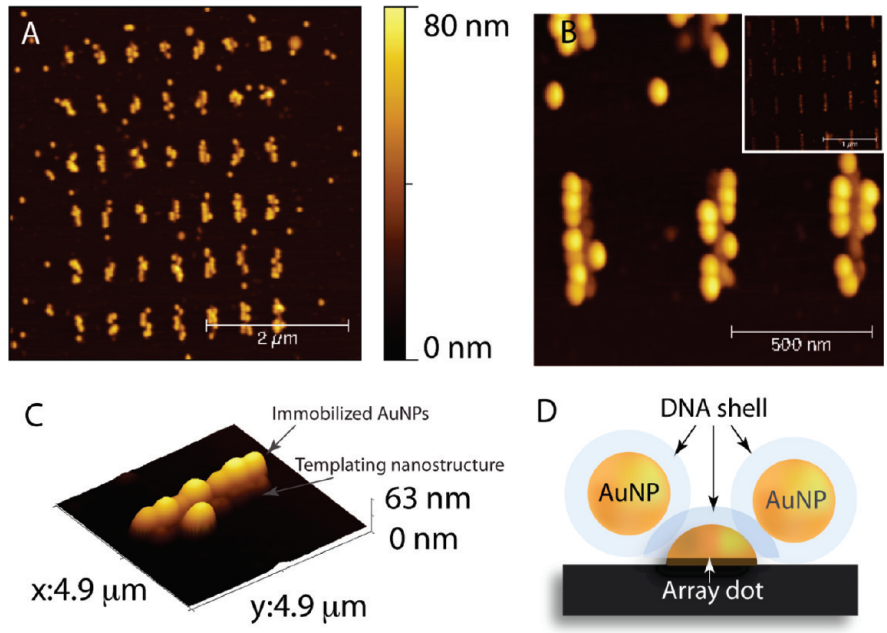

Figure 2. AFM micrographs and scheme of sub-A following the AuNP self-assembly process (the color-height bar applies to A and B including the inset): (A) successful hybridization of DNA-capped AuNPs, (B) close-ups of a few six-dot lines, the inset shows the negative control assembled onto a nanopattern carrying surface DNA but no linker, (C) three-dimensional representation of one templating nanostructure with assembled AuNPs, visualizing how the AuNPs adsorb to the side of the array, and (D) schematic illustration of the lateral adsorption of AuNPs onto the lithography defined templating structure.

was estimated to be 15−18 nm (~5 and ~12 nm Cr and Au, respectively), and the depth of the holes of sub-B was estimated to be between 4 and 6 nm (~2 and 6 nm Cr and Au, respectively). The templating nanostructures were spaced roughly 500 nm apart in the *x*-direction and 220 nm in *y*-direction (center-to-center). Typical AFM micrographs depicting sub-A following the bottom-up self-assembly of AuNPs are displayed in Figure 2.

As seen in Figure 2, the AuNPs adsorbed to the nanopattern at high yield. When the AuNP self-assembly process was conducted without linker DNA (omitting step 5 in the self-assembly process illustrated in Scheme 1), no immobilization of AuNPs was observed (inset in Figure 2B), demonstrating that the self-assembly was entirely DNA-driven. Although the immobilization efficiency was high and the assembly clearly DNA driven, the AuNPs did not immobilize straight onto the six-dot lines, and thus the immobilized AuNPs did not reproduce the templating nanopattern well. Instead the particles appeared to laterally adsorb to the lithography defined templating nanostructure, forming double lines. In Figure 2B a close-up of a few six-dot lines with assembled AuNPs are displayed; in these images the templating nanostructure (darker shaded six-dot lines) and AuNPs (brighter round spots) can be visibly distinguished, clearly displaying that the AuNPs preferably adsorbed to the side of the nanopattern. In the AFM micrograph shown in Figure 2C, a three-dimensional representation of one templating nanostructure with immobilized AuNPs, the lateral adsorption to the templating structure is very clearly visualized. The immobilization onto the nanopattern occurred in a nonregular manner, consequently a strong variation in the number of particles per six-dot line as well as their adsorption location onto the distinct dots was observed. The elevated geometry of the nanopattern allowed for the binding of multiple AuNPs from different angles, schematically illustrated in Figure 2D. It was observed that higher DNA (surface and linker) and AuNPs concentrations favored the simultaneous adsorption to both sides of the six-dot lines (Supporting Information, Figure SI-3). When conducting the surface and linker DNA hybridization step in DNA solutions of lower concentration and the AuNP immobilization step in more dilute AuNP−DNA conjugate solution, the occurrence of lateral adsorption to the nanostructure was somewhat decreased. The main problem of the lateral adsorption however prevailed, as it was due to the geometry of the templating structures rather than the AuNP self-assembly process.

Due to the observations made for the self-assembly of AuNPs onto sub-A, an alternative templating nanopattern architecture was developed, with the intention to decrease the number of possible adsorption sites on each array dot (sub-B; fabrication described above, depicted in Figure 1C and D). A 1 × 1 mm area was patterned to facilitate the statistical analysis of the AuNP self-assembly process. Typical SEM micrographs of sub-B following the self-assembly procedure are shown in Figure 3.

The self-assembled AuNPs were found to closely reproduce the underlying templating nanopattern structure over the entire patterned area. Unprecedented

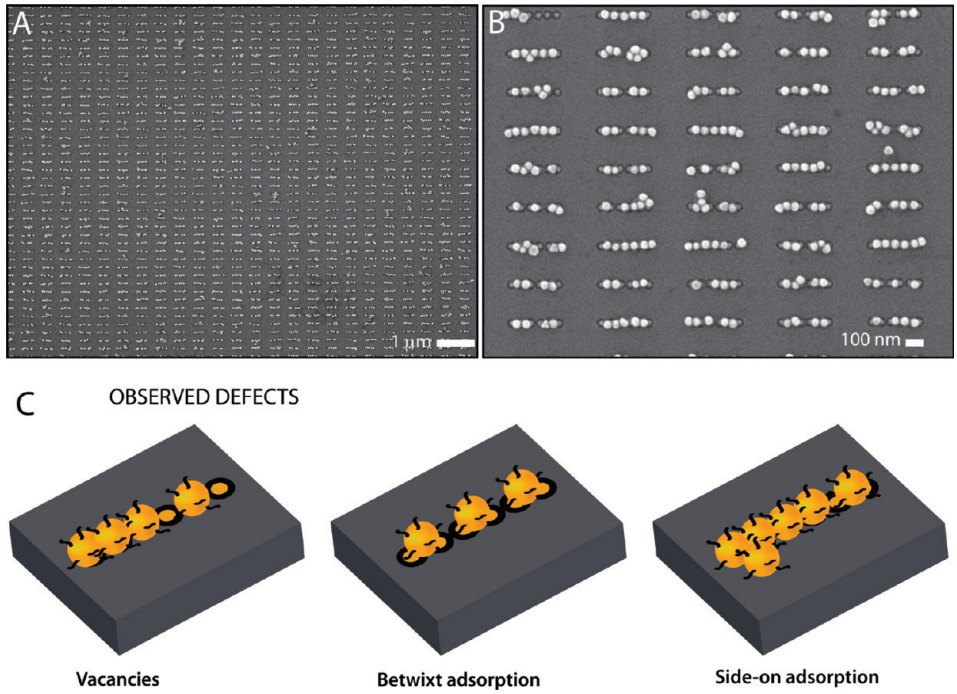

Figure 3. SEM micrographs and schemes of sub-B following the AuNP self-assembly process: (A) large area SEM micrograph of the nanopatterned following the AuNP self-assembly process, (B) close-up of selected six-dot lines, and C) schematic illustrations of observed defects in assembly configurations, namely, vacant adsorption sites, between adsorption (in between two intended adsorption sites), and side-on adsorption.

control over the DNA-directed assembly of individual nanoparticles onto lithographically defined nanopatterns could be achieved, demonstrating the feasibility to place individual nanometer-sized building blocks into precise positions within lithographically defined structures. No particle immobilization was observed in a control experiment (Figure SI-4), where the assembly process was conducted with templating nanostructures that carried surface DNA but no linker DNA, indicating that the observed assembly was directed by DNA hybridization. Figure 3B shows a close-up of a representative area within the nanopattern.

The probability of an adsorption site being occupied was 80%. This was determined by counting the total number of vacant adsorption sites found on a 10 × 9 μm area on the substrate depicted in Figure 3A, and comparing it to the total number of adsorption sites (Supporting Information, Table SI-1). The total number of nonspecifically adsorbed AuNPs (no contact with any array) on this area was 34, which amounted for 0.72% of the total number of AuNPs, an exceptionally low number.

While the templating linear six-particle arrangement was well reproduced by the self-assembled particles; certain assembly irregularities ('defects') were observed. These are schematically depicted in Figure 3C. Three major defect types were observed: (1) adsorption sites which were not occupied by AuNPs (vacancies), (2) between adsorption of nanoparticles, simultaneously bridging two individual adsorption sites, and (3) the side-on adsorption, where nanoparticles adsorb laterally to already immobilized particles.

The number of AuNPs immobilized onto each six-dot line was determined from a typical TEM image (Supporting Information, Figure SI-5), and the statistical distribution, based on the assessment of 922 assemblies, is shown in Figure 4. Close to 50% of all six-dot lines had 5 AuNPs immobilized, and in more than 98% of all six-dot lines, 4−7 AuNPs were adsorbed. Of all the six-dot lines, 20% had a total of 6 AuNPs immobilized.

The assemblies were further divided into three categories: (1) uninterrupted and (2) interrupted lines and (3) lines with side adsorption. All assemblies with particles not immediately onto the templating nanostruc-

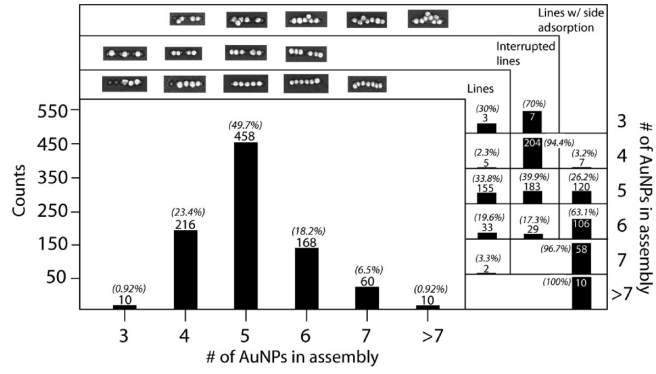

Figure 4. Chart displaying the distribution of the number of particles encompassed in assemblies divided into assembly groups of 3−7 and >7 particles. The distribution of the assembly configurations (lines, interrupted lines, and lines with side adsorption) for each assembly group is displayed to the right. The 14 assembly subcategories observed are depicted at the top of the chart.

ture were categorized into group 3, even if they were further defected, *i.e.*, an assembly immobilized into an interrupted line with side-on adsorption was classified into group 3 solely. The statistical analysis showed that for six-dot lines with five or less AuNPs within the assembly, the interrupted line configuration was the most common, while for assemblies that carried six and more AuNPs, lines with side-adsorption were most commonly observed. A total of 19.6% of all assemblies that featured six adsorbed AuNPs exhibited the aspired arrangement of six AuNPs in a linear configuration, perfectly reproducing the templating structure of the nanopattern.

Few six-dot lines had four or less particles immobilized in an uninterrupted line, still the number of six-dot lines with four AuNPs immobilized was very high. These assemblies were almost exclusively arranged in an interrupted line and were the result of the between adsorption defect, illustrated in Figure 3. This was also the case for six-dot lines with five AuNPs assembled. Of all the six-dot lines, only the ones with five AuNPs immobilized contain a significant number configured into an uninterrupted line (33.8%). If the AuNPs assemble in between the indented adsorption sites (between adsorption), five can "fit" onto the templating nanostructure. For six particles to sit in a straight line on the nanostructure, the particles must immobilize straight onto the dots of the six-dot lines (*i.e.*, onto the intended adsorption site). The geometry of these templating nanostructures appeared to favor between adsorption. This is believed due to the geometry of the six-dot lines. The isotropic wet chemical-etching process used here results in the removal of a significant amount of SiO_2 in the areas between the six adsorption sites. This is illustrated by the cross-sectional analysis shown in Figure 1D, revealing six (gold) adsorption sites as local maxima; however, these appear not to be separated by a detectable SiO_2 barrier. This thermodynamically favors the simultaneous binding to two adjacent adsorption sites in a between fashion.[54] Additional experiments (Supporting Information, Figures SI-6 and SI-7) suggested that the side-on adsorption was a consequence of the combined linker/surface DNA length, allowing for the sticky-end section of the linker DNA to stretch beyond the templating nanostructure. Deeper holes reduced the occurrence of side-on adsorption, thus it is believed that a shorter DNA strand, possibly in conjunction with carefully controlled increase in hole depth, would suppress the recurrence of the side-on adsorption defect. A high hybridization efficiency of AuNPs was observed onto individual adsorption sites (80%). As opposed to the observations made by Zhang *et al.*,[50] the drop in efficiency was not due to interparticle repulsion but a result of AuNPs being sterically hindered from adsorbing onto spatially confined adsorption sites, located at interjacent sites between two already adsorbed particles. For the self-assembling AuNPs to perfectly reproduce the templating nanostructure, the geometry of the six-dot lines should be modified; the diameter of the dot could be decreased, the center-to-center pitch distance slightly increased, and the hole depth increased (with anisotropic etching methods). This would prevent the between adsorption from occurring, while also dramatically lowering the recurrence of side-on adsorption.

CONCLUSION

We have studied the templated assembly of DNA-capped gold nanoparticles (AuNPs) onto surface nanopatterns fabricated by electron beam lithography (EBL) with the aim to control the assembly of individual nanoparticles into discrete arrays. The templating structure was composed of 6 metal patches of 36 nm diameter and a center-to-center distance of 55 nm, encoding adsorption sites for 6 individual nanoparticles. In an initial attempt, the gold surface patterns were fabricated by simple EBL/lift-off techniques, yielding elevated gold patterns of approximately 20 nm height. The DNA-directed adsorption of several AuNPs from different angles to the same surface site could be observed. As a result the array of self-assembled AuNPs did not represent a good match to the underlying nanostructure. In order to reduce the possible adsorption angles an additional wet chemical-etching step was included in the template fabrication process. As a result, gold surface nanopatterns template with negative surface features could be fabricated. DNA-directed self-assembly of AuNPs onto these templates yielded particle assemblies that reproduced the nanofeatures of these lithographically defined nanopatterns with unprecedented accuracy. The efficiency of binding AuNPs onto individual absorption sites was found to be 80%. Less than 1% of all surface confined nanoparticles was adsorbed nonspecifically in areas between the self-assembled regular arrays. Different types of assembly defects were indentified, which are believed to be a consequence of the specific template geometry that results from the isotropic wet chemical-etching step applied. Replacing this procedure with an anisotropic reactive ion-etching process should allow fabricating recessed gold structures, separated by intact areas of unetched silicon. This improved architecture would allow to avoid the between adsorption which represents the most common defect observed in this study. A number of additional factors influence the assembly yield, and their further optimization is likely to afford strong improvements in the assembly yield and the suppression of defect formation. This could pave the way toward the integration of complex nanometer building blocks into optical and electronic circuits through self-assembly, yielding complex structures with unique optical and electronic properties not attainable through any other fabrication strategy. Such building blocks can be produced in bulk quantities with sub-nm features and high structural complexity through chemical synthesis. Additional

functionalities can be conferred to such building blocks through their conjugation with molecular functionalities with particular biological, electrical, and optical properties. Alternative assembly strategies, such as electrostatic self-assembly, are currently being investigated for applications where the DNA surface capping is likely to hinder, *e.g.*, the electronic addressing of the self-assembled nanostructures.

METHODS

Synthesis of AuNP−DNA Conjugates. AuNP solution (Ted Pella, OD1, 1 mL, as received) was placed in a microcentrifuge tube and centrifuged at 3800 rpm for 40 min. The supernatant was disposed off, and a 100 μM oligonucleotide (Fidelity Systems) solution (10 μL particle DNA: 3′-$[HS]_3$-T_{15}-TAA TCA GCG TCA TAA-5′) was added to the AuNP solution, resulting in a ratio of 1160:1 ssDNA: AuNPs. The mixture was gently mixed with a vortexer (200 rpm) for approximately 2 h at room temperature (RT), upon which 140 μL ultra pure water (Barnstead NANOpure Ultrapure system), 250 μL buffer III (40 mM K_2HPO_4/KH_2PO_4, 10 mM EDTA, 0.1% tween 20), 50 μL 5 M NaCl, and 5 μL 100 mM bis(*p*-sulfonateophenyl)phenylphosphine dihydrate dipotassium (BSPP, Sigma-Aldrich) were added dropwise to the mixture and left at RT for 1 h. Incubated at RT overnight and thereafter, the excess DNA was washed off by adding 1 mL of NANOpure water and centrifuging the mixture for 40 min at 3800 rpm. The supernatant was disposed off, and the procedure was repeated twice. After the final cleaning step, 80 μL of buffer II was added, and the mixture was kept in the refrigerator, where it was stable for months. The absorption spectra show the characteristic plasmon absorption peak at 527 nm for 40 nm particles. The concentration of the AuNP−DNA conjugate solutions was calculated to be 1.4 nM by assuming an extinction coefficient (ε) of 6.7×10^9 $M^{-1}cm^{-1}$ (product information, Ted Pella), and ε does not change drastically for AuNPs upon DNA functionalization.

Nanopattern Fabrication. A 50 nm layer of poly(methyl methacrylate) (PMMA) was spin coated onto a (101) silicon substrate (1% PMMA 950 in chlorobenzene, 2000 rpm). Electron beam lithography (EBL) was conducted using a VISTECH VB300 EBL system. The pattern was then developed for 100 s in a mixture of cold (−5 °C) isopropanol:water (7:3) placed in a sonication bath). For sub-A vacuum depositions of chromium (5 nm) and gold (12 nm) were carried out using an Edwards 501 evaporator inside a glovebox. Samples were placed on a rotating tray with a source to substrate distance of 25 cm. Deposition rates and film thicknesses were measured using a calibrated quartz thickness monitor inside the vacuum chamber and were evaporated from open tungsten boats (RD Mathis, ME8 0.005 W) at a vacuum of less than 5×10^{-6} mbar. The deposition rate for both Cr and Au were 0.01−0.02 nm/s. For sub-B, the substrate was immersed into EtOH for 20 s prior to immersing into a 10% NH_4HF_2 in NANOpure water for 15 s, rinsed with NANOpure water, and dried before evaporation. Vacuum deposition was carried out using a custom-made evaporator from LB Equipment. The substrates were placed onto a nonrotating substrate holder, with a substrate to source distance of 32 cm. Deposition rate and film thickness were monitored using a quartz thickness monitor inside the chamber, and the metals were evaporated from open tungsten boats (RD Mathis, S9A 0.005 W) at a vacuum less than 2×10^{-7} Torr. A 2 nm Cr and a 6 nm Au layer were deposited at a rate of 0.01 nm/s. For both sub-A and sub-B, the PMMA was removed by immersing the samples in 1,2-dichloroethane (DCE, Sigma-Aldrich) and placing them in an ultrasonic bath for 1−5 min. The procedure was repeated three times. In order to minimize the nonspecific adsorption of the DNA-tagged AuNPs, the silicon surface was modified with 2-[methoxy(polyethyleneoxy)propyl]-trimethoxysilane (PEG-silane, Gelest Inc.). Then 1.2 μL PEG−silane, 1.2 mL toluene, and 1 μL 32% hydrochloric acid (HCl, Sigma Aldrich) were mixed in a microcentrifuge tube, and 1 mL of the mixed solution was taken out, and placed into a clean beaker. The samples were immersed into the solution and left at RT for 1 h. Following the surface modification step, the samples were washed with toluene (three times) and ethanol (twice) and were thereafter dried under a stream of nitrogen.

DNA Modifications. In a typical experiment, a 10 μL solution of surface DNA (5′-$[HS]_3$-T_{15}-TTA TGA CCC TGA TTA-3′) was prepared in buffer I. A 20 μL solution of reducing gel (PIERCE, Immobilized TCEP Disulfide Reducing Gel) was washed twice with buffer I (0.5 NaCl, 20 mM K_2HPO_4/KH_2PO_4, pH = 7) by centrifuging and disposing the supernatant, the DNA-solution was added, and the suspension left at RT for 1 h. The substrates were placed in a hybridization chamber (HC, Corning Incorporated), and a 10 μL drop of the surface DNA solution was placed onto the sample. Incubated at RT overnight. The substrates were then placed in a microcentrifuge tube filled with buffer I and mixed with a vortexer for 10 s. The buffer was replaced with fresh buffer, and this process was repeated twice. A solution of linker DNA (5′-ATT AGT CGC AGT ATT TAA TCA GGG TCA TAA-3′) was prepared in buffer I. Excess liquid was dried off the sample with a lint-free paper towel (Kimwipes) by tipping the sample edge to the tissue, making use of capillary force. Sub-A was placed back into the HC, and a 10 μL drop of the linker solution was placed onto the substrate. Sub-B was placed into a temperature-controlled hybridization chamber (TC, Eppendorf Thermomixer comfort), at 64 °C, and a 20 μL drop of the linker solution was placed onto the substrate, incubated at 64 °C for 3 min, whereupon the temperature was decreased to 25 °C over 10 min. After a 4−12 h incubation period, the substrates were placed in a microcentrifuge tube filled with buffer I and mixed with a vortexer for 10 s. The buffer was replaced with fresh buffer, and this process was repeated twice.

AuNP−DNA Conjugate Assembly onto Nanopattern Template. The excess liquid was dried off the sample with a lint-free paper towel (Kimwipes) by tipping the sample edge to the tissue, making use of capillary force. Sub-A was placed in a HC, and a 10 μL drop of the AuNP−DNA conjugate mixture was placed onto the substrate. After an incubation period of 2−2.5 h the substrate was placed in a microcentrifuge tube filled with buffer II (0.5 NaCl, 20 mM K_2HPO_4/KH_2PO_4, 5 mM EDTA, 0.05% tween 20). The AuNP−DNA conjugate mixture was placed in a round-bottom flask, and sub-B was immersed. The flask was placed in a 42−44 °C water bath that was allowed to slowly reach RT and incubated for 12 h, upon which the substrate was placed in a microcentrifuge tube filled with buffer II.

The final substrate cleaning process: a small beaker was filled with buffer II (beaker 1), and another beaker was filled with 0.1 M ammonium acetate (beaker 2). The substrates were first immersed in beaker 1, gently swirled around, and then immersed in beaker 2 (to remove salt traces). The edge of the sample was brought into contact with a lint-free paper towel (Kimwipes), using capillary force to dry the sample. The sample was kept at a tilted angle in air until completely dry.

Characterization. The samples were characterized using an Atomic Force Microscope (AFM) from Agilent Technologies (5500 AFM). Nanoworld's high-frequency non-contact probes with aluminum coating for enhanced reflectivity (NCHR), with a typical resonance frequency of 320 kHz and a force constant of 42 N/m, were used for imaging.

Acknowledgment. The authors would like to thank the Australian Research Council for their generous financial support by providing an Australian Research Fellowship as well as project (DP DP0665223) and equipment support (LE0883019) to U.B. as well as for the provision of lab space through the ARC Centre of Excellence for Electromaterials Science (ACES). The authors would also like to thank S. Watkins (Commonwealth Scientific and Industrial Research Organisation, CSIRO, Australia), S. Hsiao (Monash University), T. Bus (University of California, Berkeley), and B. Harteneck (Lawrence Berkeley National Laboratories, Berkeley) for experimental assistance. The authors would further like to ex-

press their special thanks to the Molecular Foundry (Lawrence Berkeley National Laboratories, Berkeley) for generously supporting this project by providing free access to its facilities (user projects 142: DNA-directed nanofabrication). The authors, moreover, acknowledge use of facilities within the Monash Center for Electron Microscopy and the Centers provision of scientific and technical assistance. Finally, the authors would like to acknowledge the ARC for providing equipment support through LIEF (LE0883019).

Supporting Information Available: AFM and SEM micrographs showing additional self-assembly conditions and a more detailed description of the hybridization efficiency determination. This material is available free of charge *via* the Internet at http://pubs.acs.org.

REFERENCES AND NOTES

1. Packan, P. A. Pushing the Limits. *Science* **1999**, *285*, 2079–2081.
2. Maruccio, G.; Cingolani, R.; Rinaldi, R. Projecting the Nanoworld: Concepts, Results and Perspectives of Molecular Electronics. *J. Mater. Chem.* **2004**, *14*, 542–554.
3. Elemans, J. A. A. W.; Rowan, A. E.; Nolte, R. J. M. Mastering Molecular Matter. Supramolecular Architectures by Hierarchical Self-Assembly. *J. Mater. Chem.* **2003**, *13*, 2661–2670.
4. Gates, B. D.; Xu, Q.; Stewart, M.; Ryan, D.; Willson, C. G.; Whitesides, G. M. New Approaches to Nanofabrication: Molding, Printing, and Other Techniques. *Chem. Rev.* **2005**, *105*, 1171–1196.
5. Liz-Marzan, L. M.; Giersig, M.; Mulvaney, P. Synthesis of Nanosized Gold-Silica Core-Shell Particles. *Langmuir* **1996**, *12*, 4329–4335.
6. Demers, L. M.; Park, S. J.; Taton, A. T.; Li, Z.; Mirkin, C. Orthogonal Assembly of Nanoparticles Building Blocks on Dip-Pen Nanolithographically Generated Templates of DNA. *Angew. Chem., Int. Ed.* **2001**, *40*, 3071–3073.
7. Chung, S. W.; Ginger, D. S.; Morales, M. W.; Zhang, Z.; Chandrasekhar, V.; Ratner, M. A.; Mirkin, C. A. Top-Down Meets Bottom-Up: Dip-Pen Nanolithography and DNA-Directed Assembly of Nanoscale Electrical Circuits. *Small* **2005**, *1*, 64–69.
8. Plutowski, U.; Jester, S. S.; Lenhert, S.; Kappes, M. M.; Richert, C. DNA-Based Self-Sorting of Nanoparticles on Gold Surfaces. *Adv. Mater.* **2007**, *19*, 1951–1956.
9. Kiehl, R. A. In *DNA-Directed Assembly of Nanocomponents for Nanoelectronics, Nanophotonics, and Nanosensing, Nanomaterials Synthesis, Interfacing, and Integrating in Devices, Circuits, and Systems II*; SPIE: Boston, MA, 2007; pp 67680Z−7.
10. Spatz, J. P.; Chan, V. Z. H.; Möβmer, S.; Kamm, F. M.; Plettl, A.; Ziemann, P.; Möller, M. A Combined Top-Down/Bottom-Up Approach to the Microscopic Localization of Metallic Nanodots. *Adv. Mater.* **2002**, *14*, 1827–1832.
11. Kershner, R. J.; Bozano, L. D.; Micheel, C. M.; Hung, A. M.; Fornof, A. R.; Cha, J. N.; Rettner, C. T.; Bersani, M.; Frommer, J.; Rothemund, P. W. K.; Wallraff, G. M. Placement and Orientation of Individual DNA Shapes on Lithographically Patterned Surfaces. *Nat. Nanotechnol.* **2009**, *4*, 557–561.
12. Shipway, A. N. A.; Katz, E.; Willner, I. Nanoparticle Arrays on Surfaces for Electronic, Optical, and Sensor Applications. *ChemPhysChem* **2000**, *1*, 18–52.
13. Daniel, M.-C.; Astruc, D. Gold Nanoparticles: Assembly, Supramolecular Chemistry, Quantum-Size-Related Properties, and Applications toward Biology, Catalysis, and Nanotechnology. *Chem. Rev.* **2004**, *104*, 293–346.
14. Hoeppener, S.; Maoz, R.; Cohen, S. R.; Chi, L. F.; Fuchs, H.; Sagiv, J. Metal Nanoparticles, Nanowires, and Contact Electrodes Self-Assembled on Patterned Monolayer Templates-A Bottom-up Chemical Approach. *Adv. Mater.* **2002**, *14*, 1036–1041.
15. Kelly, K. L.; Coronado, E.; Zhao, L. L.; Schatz, G. C. The Optical Properties of Metal Nanoparticles: The Influence of Size, Shape, and Dielectric Environment. *J. Phys. Chem. B* **2002**, *107*, 668–677.
16. Ditlbacher, H.; Hohenau, A.; Wagner, D.; Kreibig, U.; Rogers, M.; Hofer, F.; Aussenegg, F. R.; Krenn, J. R. Silver Nanowires as Surface Plasmon Resonators. *Phys. Rev. Lett.* **2005**, *95*, 257403.
17. Laroche, T.; Vial, A.; Roussey, M. Crystalline Structure's Influence on the Near-Field Optical Properties of Single Plasmonic Nanowires. *Appl. Phys. Lett.* **2007**, *91*, 123101.
18. Orendorff, C. J.; Gole, A.; Sau, T. K.; Murphy, C. J. Surface-Enhanced Raman Spectroscopy of Self-Assembled Monolayers: Sandwich Architecture and Nanoparticle Shape Dependence. *Anal. Chem.* **2005**, *77*, 3261–3266.
19. Schneider, G.; Decher, G. From Functional Core/Shell Nanoparticles Prepared Via Layer-By-Layer Deposition to Empty Nanospheres. *Nano Lett.* **2004**, *4*, 1833–1839.
20. Xie, J.; Zhang, Q.; Lee, J. Y.; Wang, D. I. C. The Synthesis of SERS-Active Gold Nanoflower Tags for In Vivo Applications. *ACS Nano* **2008**, *2* (12), 2473–2480.
21. Ellenborgen, J. C. In *A Brief Overview of Nanoelectronic Devices*, Proceedings of the Government Microelectronics Applications Conference (GOMAC98), Arlington, VA, March 13−16, 1998; The MITRE Corporation: Arlington, VA, 1998; pp 1−5.
22. Goldhaber-Gordon, D.; Montemerlo, M. S.; Love, J. C.; Opiteck, G. J.; Ellenbogen, J. C. Overview of Nanoelectronic Devices. *Proc. IEEE* **1997**, *85*, 521–540.
23. Klein, D. L.; Roth, R.; Lim, A. K. L.; Alivisatos, A. P.; McEuen, P. L. A Single-Electron Transistor Made from a Cadmium Selenide Nanocrystal. *Nature* **1997**, *389*, 699–701.
24. Huynh, W. U.; Peng, X. A.; Alivisatos, P. CdSe Nanocrystal Rods/Poly(3-hexylthiophene) Composite Photovoltaic Devices. *Adv. Mater.* **1999**, *11*, 923–927.
25. Milliron, D. J.; Hughes, S. M.; Cui, Y.; Manna, L.; Li, J.; Wang, L.-W.; Paul Alivisatos, A. Colloidal Nanocrystal Heterostructures with Linear and Branched Topology. *Nature* **2004**, *430*, 190–195.
26. Fu, A.; Micheel, C. M.; Cha, J.; Chang, H.; Yang, H.; Alivisatos, A. P. Discrete Nanostructures of Quantum Dots/Au with DNA. *J. Am. Chem. Soc.* **2004**, *126*, 10832–10833.
27. Claridge, S. A.; Goh, S. L.; Frechet, J. M. J.; Williams, S. C.; Micheel, C. M.; Alivisatos, A. P. Directed Assembly of Discrete Gold Nanoparticle Groupings Using Branched DNA Scaffolds. *Chem. Mater.* **2005**, *17*, 1628–1635.
28. Yoo, B. S.; Liu, X. C.; Petrou, A.; Cheng, J. P.; Reeder, A. A.; McCombe, B. D.; Elcess, K.; Fonstad, C. Optical and Infrared Studies of [111] InGaAs/AlGaAs Strained-Layer Superlattices. *Superlattices Microstruct.* **1989**, *5*, 363–366.
29. Maye, M. M.; Kumara, M. T.; Nykypanchuk, D.; Sherman, W. B.; Gang, O. Switching Binary States of Nanoparticle Superlattices and Dimer Clusters by DNA Strands. *Nat. Nanotechnol.* **2010**, *5*, 116–120.
30. Cardenas, M.; Barauskas, J.; Schillen, K.; Brennan, J. L.; Brust, M.; Nylander, T. Thiol-Specific and Nonspecific Interactions between DNA and Gold Nanoparticles. *Langmuir* **2006**, *22*, 3294–3299.
31. Qiu, F.; Jiang, D.; Ding, Y.; Zhu, J.; Huang Lequn, L. Monolayer-Barcoded Nanoparticles for On-Chip DNA Hybridization Assay. *Angew. Chem., Int. Ed.* **2008**, *47*, 5009–5012.
32. Mastroianni, A. J.; Claridge, S. A.; Alivisatos, A. P. Pyramidal and Chiral Groupings of Gold Nanocrystals Assembled Using DNA Scaffolds. *J. Am. Chem. Soc.* **2009**, *131*, 8455–8459.
33. Link, S.; El-Sayed, M. A. Spectral Properties and Relaxation Dynamics of Surface Plasmon Electronic Oscillations in Gold and Silver Nanodots and Nanorods. *J. Phys. Chem. B* **1999**, *103*, 8410–8426.
34. Sönnichsen, C.; Geier, S.; Hecker, N. E.; von Plessen, G.; Feldmann, J.; Ditlbacher, H.; Lamprecht, B.; Krenn, J. R.; Aussenegg, F. R.; Chan, V. Z. H.,; *et al.* Spectroscopy of Single Metallic Nanoparticles Using Total Internal Reflection Microscopy. *Appl. Phys. Lett.* **2000**, *77*, 2949–2951.
35. Su, K. H.; Wei, Q. H.; Zhang, X.; Mock, J. J.; Smith, D. R.;

Schultz, S. Interparticle Coupling Effects on Plasmon Resonances of Nanogold Particles. *Nano Lett.* **2003**, *3*, 1087–1090.
36. Maier, S. A.; Atwater, H. A. Plasmonics: Localization and Guiding of Electromagnetic Energy in Metal/Dielectric Structures. *J. Appl. Phys.* **2005**, *98*, 011101.
37. Rechberger, W.; Hohenau, A.; Leitner, A.; Krenn, J. R.; Lamprecht, B.; Aussenegg, F. R. Optical Properties of Two Interacting Gold Nanoparticles. *Opt. Commun.* **2003**, *220*, 137–141.
38. Sönnichsen, C.; Reinhard, B. M.; Liphardt, J.; Alivisatos, A. P. A Molecular Ruler Based on Plasmon Coupling of Single Gold and Silver Nanoparticles. *Nat. Biotechnol.* **2005**, *23*, 741–745.
39. Liu, S. T.; Maoz, R.; Sagiv, J. Planned Nanostructures of Colloidal Gold via Self-assembly on Hierarchically Assembled Organic Bilayer Template Patterns with In-situ Generated Terminal Amino Functionality. *Nano Lett.* **2004**, *4*, 845–851.
40. Khatri, O. P.; Han, J.; Ichii, T.; Murase, K.; Sugimura, H. Self-assembly Guided One-Dimensional Arrangement of Gold Nanoparticles: A Facile Approach. *J. Phys. Chem. C* **2008**, *112*, 16182–16185.
41. Li, B.; Lu, G.; Zhou, X. Z.; Cao, X. H.; Boey, F.; Zhang, H. Controlled Assembly of Gold Nanoparticles and Graphene Oxide Sheets on Dip Pen Nanolithography-Generated Templates. *Langmuir* **2009**, *25*, 10455–10458.
42. Liu, S. T.; Maoz, R.; Schmid, G.; Sagiv, J. Template Guided Self-assembly of [Au55] Clusters on Nanolithographically Defined Monolayer Patterns. *Nano Lett.* **2002**, *2*, 1055–1060.
43. Hung, A. M.; Micheel, C. M.; Bozano, L. D.; Osterbur, L. W.; Wallraff, G. M.; Cha, J. N. Large-Area Spatially Ordered Arrays of Gold Nanoparticles Directed by Lithographically Confined DNA Origami. *Nat. Nanotechnol.* **2010**, *5*, 121–126.
44. Ofir, Y.; Samanta, B.; Xiao, Q.; Jordan, B. J.; Xu, H.; Arumugam, P.; Arvizo, R.; Tuominen, M. T.; Rotello, V. M. Electrostatic Assembly of Nanoparticles and Electroless Deposition of Metallic Films. *Adv. Mater.* **2008**, *20*, 2561–2566.
45. Alivisatos, A. P.; Johnsson, K. P.; Peng, X.; Wilson, T. E.; Loweth, C. J.; Bruchez, M. P.; Schultz, P. G. Organization of 'Nanocrystal Molecules' Using DNA. *Nature* **1996**, *382*, 609–611.
46. Mirkin, C. A.; Letsinger, R. L.; Mucic, R. C.; Storhoff, J. J. A DNA-Based Method for Rationally Assembling Nanoparticles into Macroscopic Materials. *Nature* **1996**, *382*, 607–609.
47. Loweth, C. J.; Caldwell, W. B.; Peng, X.; Alivisatos, A. P.; Schultz, P. G. DNA-Based Assembly of Gold Nanocrystals. *Angew. Chem., Int. Ed.* **1999**, *38*, 1808–1812.
48. Cho, Y.-K.; Kim, S.; Kim, Y. A.; Lim, H. K.; Lee, K.; Yoon, D.; Lim, G.; Pak, E.; Hwan, T.; Kim, K. Characterization of DNA Immobilization and Subsequent Hybridization Using In Situ Quartz Crystal Microbalance, Fluorescence Spectroscopy, and Surface Plasmon Resonance. *J. Colloid Interface Sci.* **2004**, *278*, 44–52.
49. Jaswinder, S.; Rahul, C.; Yan, L.; Yonggang, K.; Hao, Y. DNA-Templated Self-Assembly of Two-Dimensional and Periodical Gold Nanoparticle Arrays. *Angew. Chem., Int. Ed.* **2006**, *45*, 730–735.
50. Zhang, J.; Liu, Y.; Ke, Y.; Yan, H. Periodic Square-Like Gold Nanoparticle Arrays Templated by Self-Assembled 2D DNA Nanogrids on a Surface. *Nano Lett.* **2006**, *6*, 248–251.
51. Pal, S.; Sharma, J.; Yan, H.; Liu, Y. Stable Silver Nanoparticle-DNA Conjugates for Directed Self-Assembly of Core-Satellite Silver-Gold Nanoclusters. *Chem. Commun.* **2009**, 6059–6061.
52. Ding, B.; Deng, Z.; Yan, H.; Cabrini, S.; Zuckermann, R. N.; Bokor, J. Gold Nanoparticle Self-Similar Chain Structure Organized by DNA Origami. *J. Am. Chem. Soc.* **2010**, *132*, 3248–3249.
53. Sharma, J.; Chhabra, R.; Andersen, C. S.; Gothelf, K. V.; Yan, H.; Liu, Y. Toward Reliable Gold Nanoparticle Patterning On Self-Assembled DNA Nanoscaffold. *J. Am. Chem. Soc.* **2008**, *130*, 7820–7821.
54. Park, S. Y.; Lytton-Jean, A. K. R.; Lee, B.; Weigand, S.; Schatz, G. C.; Mirkin, C. A. DNA-Programmable Nanoparticle Crystallization. *Nature* **2008**, *451*, 553–556.